Spectrum of coherently backscattered light from two atoms

Vyacheslav Shatokhin,[1,2] Thomas Wellens,[3] Benoît Grémaud,[4] and Andreas Buchleitner[1]

[1] *Max-Planck-Institut für Physik komplexer Systeme, Nöthnitzer Str. 38, 01187 Dresden, Germany*
[2] *B. I. Stepanov Institute of Physics, National Academy of Sciences, Skaryna Ave. 68, 220072 Minsk, Belarus*
[3] *Institut für Theoretische Physik, Universität Erlangen-Nürnberg, Staudstr. 7, 91058 Erlangen, Germany*
[4] *Laboratoire Kastler Brossel, Université Pierre et Marie Curie, 4, place Jussieu, 75252 Paris Cedex 05, France*

(Dated: February 2, 2008)

We present a detailed analytical and numerical analysis of the inelastic coherent backscattering spectrum of laser light incident on cold atoms. We identify frequency domains where the interference contribution can be positive as well as negative – or exhibits dispersive character. These distinctive features are explained by reciprocity arguments and dressed state two-photon scattering amplitudes.

PACS numbers:

I. INTRODUCTION

Multiple scattering of light in cold atomic gases has become an area of intense theoretical and experimental research (for a recent review, see [1]). On the experimental side, the successful observation of coherent backscattering (CBS) of light in clouds of cold atoms [2, 3] demonstrated the potential of finely tunable atomic media for detailed studies of localization and transport phenomena [4] in the weak and, prospectively, strong localization regime. On the theoretical side, it is of crucial importance to understand how interference effects are affected by various dephasing mechanisms characteristic for atom-photon interactions, for ensembles of atoms cooled down to approximately 100 μK, with, in general, degenerate electronic structure, and in the presence of inelastic scattering. It is presently also realized that multiple scattering of light in atomic clouds is relevant in the context of quantum information storage and retrieval by photons, in the parameter regime of electromagnetically-induced transparency (EIT) [5]. This promotes CBS studies toward the dynamical regime [6]. Also multiple scattering of *nonclassical* light [7] is presently moving into focus.

In our present contribution, we will expand on the impact of inelastic scattering processes on CBS. Experimental studies on cold Sr atoms revealed a rapid decrease of the CBS interference contrast with increasing intensity of the injected laser field, as a consequence of the saturation of the laser-driven atomic transition [8]. A much weaker sensitivity of the quality of the CBS signal was observed for Rb atoms [9]. In this latter case, inelastic processes occur on degenerate transitions [10, 11, 12, 13, 14], while Sr atoms offer dipole transitions with a nondegenerate ground state [15].

So far, the role of the nonlinearity of the atom-photon interaction for CBS scatterers has been theoretically investigated only for Sr atoms [16, 19, 20, 21, 22]. Within a scattering theoretical approach applied to two atoms in the regime of weakly nonlinear scattering [16], the decrease of the CBS enhancement factor α was shown to be due to the partial distinguishability of the interfering amplitudes. In the general case of many atoms, three different amplitudes interfere constructively in the weakly nonlinear regime, such that α may exceed the linear barrier two [17, 18]. For arbitrary intensities of the injected laser light, a number of effects have been predicted within a master equation approach [19, 20], such as a nonvanishing residual CBS contrast in the deep saturation regime, or CBS anti-enhancement under off-resonant driving. The strongly inelastic scattering regime studied by a quantum Langevin treatment highlighted the crucial role of inelastic susceptibilities [21].

Here, we will focus on the spectral properties of the CBS signal, in order to provide a detailed interpretation of the residual CBS enhancement or anti-enhancement predicted earlier [19, 20]. This will also elucidate the structure of the CBS spectra presented in [21, 22]. Specifically, we will identify frequency domains where the interference contribution to CBS exhibits not only constructive but also destructive terms, or else a dispersive lineshape. We relate the spectral lines of the CBS spectrum to CBS transitions between atomic dressed states. We show that, in the limit of very intense laser fields, spectral ranges with destructive interference lead to a decreased enhancement factor, which, at exact resonance, shrinks to $\alpha_\infty = 23/21$. For off-resonance driving, the destructively interfering processes can outweigh the constructively interfering ones, leading to values of the enhancement factor less than unity.

The paper is organized as follows: We start with a brief presentation of our two-atom model, and of the master equation approach. In Sec. III we present our results on the CBS spectrum. Section IV concludes the paper.

II. A MASTER EQUATION FOR TWO ATOMS

A. The model, and the main quantity of interest

While details of our approach were presented elsewhere [20], we recollect its basic ingredients relevant for our subsequent spectral analysis. We start out with the general formulation of a Hamiltonian describing N identical, stationary atoms embedded in an electromagnetic environment of quantized harmonic oscillators, and subjected

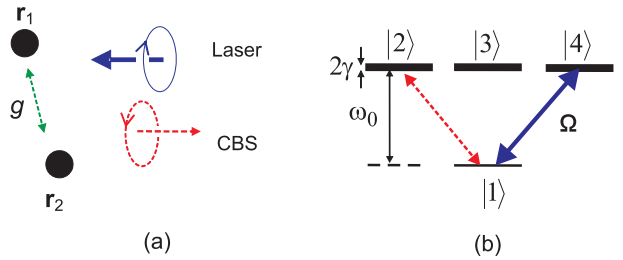

FIG. 1: Model of CBS with two atoms. (a) atoms (black dots) are driven by laser light with right circular polarization, while CBS is observed in the helicity preserving channel, that is, with flipped polarization. Photons in this channel appear as a result of double scattering. g is the strength of the far-field dipole-dipole coupling responsible for the exchange of photons; (b) internal atomic structure corresponding to a $J_g = 0 \to J_e = 1$ dipole transition. ω_0 is the transition frequency, 2γ is the radiative linewidth, Ω is the Rabi frequency. Sublevels $|1\rangle$ and $|3\rangle$ have magnetic quantum number $m = 0$. Sublevels $|2\rangle$ and $|4\rangle$ correspond to $m = -1$ and $m = 1$, respectively. The thick solid arrow represents the laser field driving the $|1\rangle \leftrightarrow |4\rangle$ transition, while the dashed arrow indicates the CBS field originating from the $|1\rangle \leftrightarrow |2\rangle$ transition.

to an external (classical) laser field of arbitrary intensity. Coupling to the bath gives rise to spontaneous emission from the excited state and to the far-field dipole-dipole interaction responsible for the exchange of photons between the atoms, whereas the coupling to the laser field induces Rabi oscillations of the populations and coherences on the laser-driven atomic transitions.

The intensity of the light scattered off the atomic system is expressed via the correlation functions of the emitting dipoles. We address a regime of multiple scattering which is relatively simple from the theoretical point of view: scattering by an optically thin atomic medium, where double scattering provides the dominant contribution to the CBS signal [10, 15]. It is in this double scattering regime where the first observation of a CBS reduction due to the saturation of atomic dipole transitions was reported [8].

Under this specific conditions, considering a system of only two atoms suffices to grasp the essential physical phenomena. Thus, we come up with the toy model of CBS depicted in Fig. 1. We will study CBS from two identical, motionless atoms, located at positions $\mathbf{r}_1$ and $\mathbf{r}_2$, with the distance $r_{12} = |\mathbf{r}_1 - \mathbf{r}_2|$ being much greater than the optical wavelength λ.

As for the internal atomic structure we choose non-degenerate atomic ground states, and the excited state with a three-fold degeneracy [see Fig. 1(b)], precisely as in the Sr experiment [8]. The laser intensity is encoded in the saturation parameter $s = \Omega^2/2(\gamma^2 + \delta^2)$, where Ω is the Rabi frequency, γ is half the spontaneous decay rate of the atomic excited states, and $\delta = \omega_L - \omega_0$ is the laser-atom detuning.

We will consider the CBS signal in the helicity preserving ($h \parallel h$) polarization channel, as in [8], with right circularly polarized laser light driving the $|1\rangle \leftrightarrow |4\rangle$ transition, that is, $\boldsymbol{\varepsilon}_L = \hat{\mathbf{e}}_{+1}$, in helicity basis notation. CBS with preserved helicity then corresponds to the detection of photons with flipped polarization, $\boldsymbol{\varepsilon} = \hat{\mathbf{e}}_{-1}$, that is, from $|1\rangle \leftrightarrow |2\rangle$ transition, as shown in Fig. 1.

The CBS spectrum can be derived from the average value of the first-order temporal correlation function of the field [23]:

$$G^{(1)}(\mathbf{r}, t; \mathbf{r}, t') = \left\langle \mathrm{Tr}\left\{\rho[\boldsymbol{\varepsilon} \cdot \mathbf{E}_{\mathrm{s}}^{(-)}(\mathbf{r}, t)][\boldsymbol{\varepsilon}^* \cdot \mathbf{E}_{\mathrm{s}}^{(+)}(\mathbf{r}, t')]\right\}\right\rangle_{\mathrm{conf}}, \tag{1}$$

where ρ is the initial density operator of the atom-field system, $\mathbf{E}_{\mathrm{s}}^{(-/+)}(\mathbf{r}, t)$ is the negative/positive frequency component of the electric field operator of the scattered field, and $\langle \ldots \rangle_{\mathrm{conf}}$ denotes a configuration average. The components of the scattered field are the retarded fields radiated by the atomic dipoles,

$$\mathbf{E}_{\mathrm{s}}^{(+)}(\mathbf{r}, t) = \frac{\omega_0^2}{4\pi\varepsilon_0 c^2 r} \sum_{\alpha=1}^{2} \mathbf{D}_\alpha(t_\alpha) e^{-i\mathbf{k}\cdot\mathbf{r}_\alpha}, \tag{2}$$

where ε_0 is the permittivity of the vacuum, $\mathbf{D}_\alpha = -\hat{\mathbf{e}}_{-1}\sigma_{12}^\alpha + \hat{\mathbf{e}}_0\sigma_{13}^\alpha - \hat{\mathbf{e}}_{+1}\sigma_{14}^\alpha$, with $\sigma_{kl}^\alpha \equiv |k\rangle_\alpha \langle l|_\alpha$, is the dipole lowering operator, and $t_\alpha = t - |\mathbf{r} - \mathbf{r}_\alpha|/c$. In writing Eq. (2), we have assumed that $r_{12} \ll r$, that is, the field is detected at a distance much larger than the interatomic distance. In the following, we will for brevity omit the r-dependent prefactor of Eq. (2) and, consistently, of the temporal correlation functions.

Inserting Eq. (2) into Eq. (1) we obtain, in the steady state limit $t \to \infty$,

$$G_{\mathrm{ss}}^{(1)}(\tau) = \sum_{\alpha,\beta=1}^{2} \langle\langle \sigma_{21}^\alpha \sigma_{12}^\beta(\tau)\rangle_{\mathrm{ss}} e^{i\mathbf{k}\cdot\mathbf{r}_{\alpha\beta}}\rangle_{\mathrm{conf}}, \tag{3}$$

where "ss" stands for *steady state*, $\tau = t' - t \geq 0$, $\mathbf{r}_{\alpha\beta} \equiv \mathbf{r}_\alpha - \mathbf{r}_\beta$, and the inner angular brackets indicate the quantum mechanical expectation value [see Eq. (1)].

The spectrum follows via a Laplace transform of (3) [24],

$$S(\nu) = \frac{1}{\pi} \lim_{\Gamma \to 0} \mathrm{Re}\left\{\tilde{G}_{\mathrm{ss}}^{(1)}(z)\right\}, \tag{4}$$

where $\tilde{G}_{\mathrm{ss}}^{(1)}(z) = \int_0^\infty d\tau \exp(-z\tau) G_{\mathrm{ss}}^{(1)}(\tau)$, $z = \Gamma - i\nu$, with $\Gamma \geq 0$, and $\nu = \omega - \omega_L$. Note that the spectrum is defined with respect to the laser frequency, what implies that the atomic correlation functions must be evaluated in the frame rotating at ω_L.

B. Configuration average

A configuration average is necessary because the two-atom correlation functions may sensitively depend on the interatomic distance, and on the orientation of the vector $\mathbf{r}_{12}$ with respect to $\mathbf{k}_L$, and thus exhibit rapid oscillations

around the backscattering direction. These oscillations have the same nature as a speckle pattern scattered off a disordered medium. After many realizations of the disorder all interference maxima except the one due to CBS disappear. A simple and sufficient way to mimic disorder in our two-atom system is to assume an isotropic distribution of the radius-vector connecting the atoms, and a uniform distribution (with a width λ) of interatomic distances around the average distance ℓ equal to the scattering mean free path.

C. Master equation

To deduce the atomic correlation functions which enter the right hand side of Eq. (3) we adapted [19, 20] the theoretical approach of [25]. Within this setting, the dynamics of the dipole operators' expectation values as well as of the dipole-dipole correlators is governed by the master equation

$$\langle \dot{Q} \rangle = \sum_{\alpha=1}^{2} \langle \mathcal{L}_\alpha Q \rangle + \sum_{\alpha \neq \beta = 1}^{2} \langle \mathcal{L}_{\alpha\beta} Q \rangle, \tag{5}$$

where the Liouvillians $\mathcal{L}_\alpha$ and $\mathcal{L}_{\alpha\beta}$ generate the time evolution of an arbitrary atomic operator Q, for independent and interacting atoms, respectively. Explicitly,

$$\begin{aligned} \mathcal{L}_\alpha Q = & -i\delta[\mathbf{D}_\alpha^\dagger \cdot \mathbf{D}_\alpha, Q] - \frac{i}{2}[\Omega_\alpha(\mathbf{D}_\alpha^\dagger \cdot \boldsymbol{\varepsilon}_L) + \Omega_\alpha^*(\mathbf{D}_\alpha \cdot \boldsymbol{\varepsilon}_L^*), Q] \\ & + \gamma(\mathbf{D}_\alpha^\dagger \cdot [Q, \mathbf{D}_\alpha] + [\mathbf{D}_\alpha^\dagger, Q] \cdot \mathbf{D}_\alpha), \end{aligned} \tag{6}$$

$$\mathcal{L}_{\alpha\beta} Q = \mathbf{D}_\alpha^\dagger \cdot \overleftrightarrow{\mathbf{T}}(g, \hat{\mathbf{n}}) \cdot [Q, \mathbf{D}_\beta] + [\mathbf{D}_\beta^\dagger, Q] \cdot \overleftrightarrow{\mathbf{T}}^*(g, \hat{\mathbf{n}}) \cdot \mathbf{D}_\alpha \,, \tag{7}$$

where $\Omega_\alpha = \Omega e^{i\mathbf{k}_L \cdot \mathbf{r}_\alpha}$ is the position-dependent Rabi frequency. The radiative dipole-dipole interaction due to exchange of photons between the atoms is described by the tensor $\overleftrightarrow{\mathbf{T}}(g, \hat{\mathbf{n}}) = \gamma g \overleftrightarrow{\boldsymbol{\Delta}}$, with $\overleftrightarrow{\boldsymbol{\Delta}} = \overleftrightarrow{\mathbb{1}} - \hat{\mathbf{n}}\hat{\mathbf{n}}$ the projector on the transverse plane defined by the unit vector $\hat{\mathbf{n}}$ along the connecting line between atoms α and β. This interaction has a certain strength, depending on the distance between the atoms, via

$$g = \frac{3i}{2k_0 r_{\alpha\beta}} e^{ik_0 r_{\alpha\beta}}, \tag{8}$$

with $k_0 = \omega_0/c$, and on the life time of the excited atomic levels, through γ. The coupling constant $|g| \ll 1$ is small in the far-field ($k_0 r_{\alpha\beta} \gg 1$), where near-field interaction terms of order $(k_0 r_{\alpha\beta})^{-2}$ and $(k_0 r_{\alpha\beta})^{-3}$ can be neglected.

Of course, an arbitrary operator Q inserted into Eq. (5) does not result in a closed differential equation. Our system consisting of two 4-level atoms leads to $255 = 4^2 \times 4^2 - 1$ linear coupled equations of motion for the associated expectation values. We solve them perturbatively to second order in g, to account for the lowest order (double-)scattering processes giving rise to a nontrivial interference contribution. To keep this in mind, symbols denoting double scattering intensities and spectra will carry the subscript 2.

Note that Eq. (5) describes the evolution of one-point correlation functions, whereas $G_{\rm ss}^{(1)}(\tau)$ is a *two*-point correlation function. By virtue of the quantum regression theorem [24], the latter also satisfies Eq. (5), with initial conditions extracted from the stationary solution of (5). In particular, the double scattering counterpart of $G_{\rm ss}^{(1)}(0)$ is nothing but the stationary average backscattered light intensity which will be referred to as $I_2^{\rm tot}$. There is an obvious relation between $I_2^{\rm tot}$ and $S_2(\nu)$ [obtained by expanding (3) to second order, in (4)]:

$$I_2^{\rm tot} = \int_{-\infty}^{\infty} d\nu S_2(\nu). \tag{9}$$

The total CBS intensity at backscattering direction can be decomposed in a sum of two terms,

$$I_2^{\rm tot} = L_2^{\rm tot} + C_2^{\rm tot}, \tag{10}$$

where $C_2^{\rm tot} \equiv C_2^{\rm tot}(\theta = 0)$ (i.e., $\mathbf{k} = -\mathbf{k}_L$), and

$$C_2^{\rm tot}(\theta) \;=\; 2\,{\rm Re}\,\langle \langle \sigma_{21}^1 \sigma_{12}^2 \rangle_{\rm ss}^{[2]} e^{i\mathbf{k}\cdot\mathbf{r}_{12}} \rangle_{\rm conf}\,, \tag{11}$$

$$L_2^{\rm tot} \;=\; \langle \langle \sigma_{22}^1 \rangle_{\rm ss}^{[2]} + \langle \sigma_{22}^2 \rangle^{[2]} \rangle_{\rm ss} \rangle_{\rm conf}\,, \tag{12}$$

are the so-called "crossed" ($C_2^{\rm tot}(\theta = 0)$) and "ladder" ($L_2^{\rm tot}$) terms, respectively. Using these, we can derive the standard measure of the phase coherence between the counterpropagating amplitudes that contribute to CBS – the enhancement factor

$$\alpha = 1 + \frac{C_2^{\rm tot}}{L_2^{\rm tot}}. \tag{13}$$

For perfect two-wave interference, $\alpha = 2$. In general, the total backscattered light intensity has elastic and inelastic components,

$$I_2^{\rm tot} = I_2^{\rm el} + I_2^{\rm inel}, \tag{14}$$

with the elastic component given by products of the expectation values of the atomic dipoles,

$$I_2^{\rm el} = \sum_{\alpha,\beta=1}^{2} \langle \langle \sigma_{21}^\alpha \rangle_{\rm ss}^{[1]} \langle \sigma_{12}^\beta \rangle_{\rm ss}^{[1]} e^{-i\mathbf{k}_L \cdot \mathbf{r}_{\alpha\beta}} \rangle_{\rm conf}. \tag{15}$$

For $\alpha = \beta$ we obtain the elastic ladder term $L_2^{\rm el}$, and for $\alpha \neq \beta$ the elastic crossed term $C_2^{\rm el}$. Given $I_2^{\rm tot}$ and $I_2^{\rm el}$, also the fluctuating part of the dipole correlation functions defining $I_2^{\rm inel}$ is determined.

A detailed derivation of the stationary CBS intensity, together with analytical results for $\delta = 0$, can be found in Appendix A.

III. CBS SPECTRUM

With the above premises, we can now proceed to the detailed analysis of the CBS spectrum, the central object

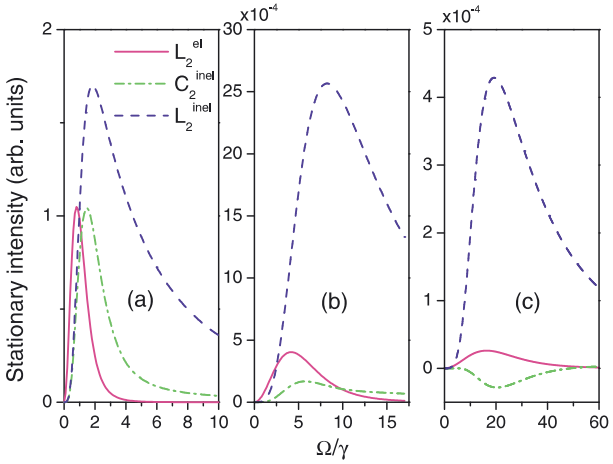

FIG. 2: (Color online) Elastic ladder, $L_2^{\rm el}$ (solid), inelastic ladder, $L_2^{\rm inel}$ (dashed), and inelastic crossed, $C_2^{\rm inel}$, (dashed-dotted) CBS contributions vs. Rabi frequency Ω, for different values of the detuning δ: $\delta =$ (a) 0; (b) 5γ; (c) 20γ.

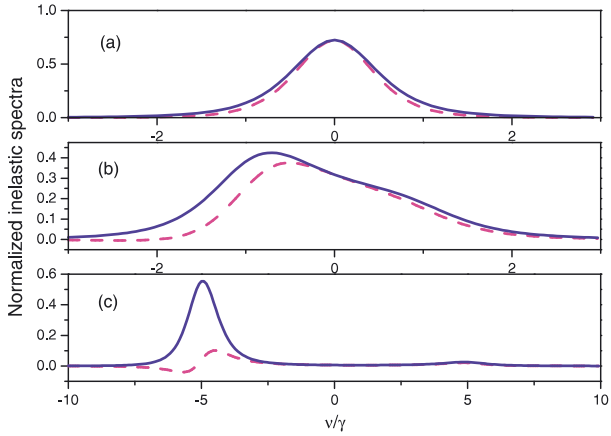

FIG. 3: (Color online) Normalized inelastic spectra of the ladder, $\tilde{L}_2^{\rm inel}(\nu)$ (solid), and crossed, $\tilde{C}_2^{\rm inel}(\nu)$ (dashed), terms at $\Omega = 0.1\gamma$. $\delta =$ (a) 0; (b) γ; (c) 5γ.

of this paper. A detailed derivation of the CBS spectrum from the solution of Eq. (5) is given in the Appendix B, while the physical content thereof will be discussed in the following sections.

A. Elastic spectrum

In the saturation regime, the double scattering spectrum of CBS has elastic and inelastic parts. The elastic spectrum in the backscattering direction reads

$$\tilde{I}_2^{\rm el}(\nu) = I_2^{\rm el}\delta(\nu), \tag{16}$$

where $\delta(\nu)$ is Dirac's delta-function, and $I_2^{\rm el} = L_2^{\rm el} + C_2^{\rm el}$, with the ladder and crossed contributions [20]

$$L_2^{\rm el} = C_2^{\rm el} = \frac{2|\bar{g}|^2}{15}\frac{1}{1+(\delta/\gamma)^2}\frac{s}{(1+s)^4}, \tag{17}$$

where $\bar{g}$ is the configuration averaged value of g. A detailed interpretation of the elastic intensity was given in previous work [19, 20]. Here, we will focus on the ...

B. Inelastic spectrum

1. Normalization

Since we are interested in the spectral properties of CBS, we will omit all frequency-independent prefactors. This is naturally achieved when considering normalized expressions. We choose the stationary inelastic ladder contribution $L_2^{\rm inel}$ as normalization factor, such that the integrals of $\tilde{L}_2^{\rm inel}(\nu)/L_2^{\rm inel}$ and $\tilde{C}_2^{\rm inel}(\nu)/L_2^{\rm inel}$ over ν yield unity and $C_2^{\rm inel}/L_2^{\rm inel}$, respectively. In the deep saturation regime, the value of the latter integral tends to the asymptotic value of the interference contrast of CBS, $\alpha_\infty(\delta) - 1$. Furthermore, for arbitrary saturation, the areas under the peaks of the normalized ladder spectrum give the relative probabilities of the corresponding inelastic processes.

The normalization itself depends on the parameters of the driving field. In Fig. 2, we present several examples of the elastic and inelastic intensities, as functions of Ω, and for different values of the detuning δ. This figure shows, in particular, that, for $\delta = 20\gamma$, the inelastic crossed term is negative, for a range of Rabi frequencies, with a minimum at $\Omega \simeq 20\gamma = \delta$ (see Fig. 2(c)). Furthermore, note that, since $C_2^{\rm el} = L_2^{\rm el}$, the total crossed term $C_2^{\rm el} + C_2^{\rm inel} < 0$ around $\Omega = 20\gamma$. The values of $C_2^{\rm el} = L_2^{\rm el}$, $C_2^{\rm inel}$, and $L_2^{\rm inel}$ at $\Omega = 20\gamma$ and $\delta = 20\gamma$ are 2.45×10^{-5}, -2.82×10^{-5}, and 4.27×10^{-4}, respectively, what implies $C_2^{\rm inel}/L_2^{\rm inel} = -0.066$, and $\alpha = 0.991$. The negativity of the total crossed term thus results in anti-enhancement (i.e., an enhancement factor $\alpha < 1$) and was reported previously [20]. It is one of the purposes of the present paper to identify the physical origin thereof.

2. Weakly inelastic scattering

In the regime of small Rabi frequencies $\Omega \ll \gamma$, it is the lowest-order inelastic processes – two-photon processes, proportional to Ω^2 – that contribute to the inelastic spectrum. Consequently, the emerging spectral features of the ladder and crossed spectra derived with the aid of the master equation approach (see Fig. 3) can be interpreted on the basis of two-photon amplitudes derived in [16]. There it was shown that, in the weakly inelastic regime, one of the two atoms must scatter inelastically. Furthermore, for direct and (time-)reversed amplitudes (which have to interfere constructively to create the CBS signal), the inelastically scattering atom must be the same. Then it turns out that, although initial and

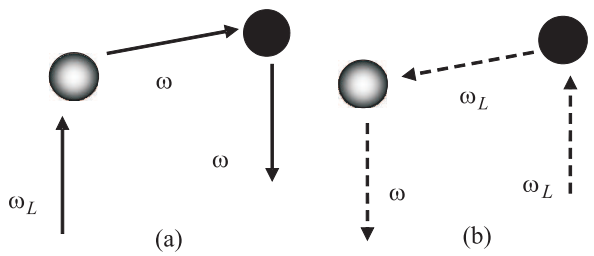

FIG. 4: Direct (a) and (time-)reversed (b) scattering paths/amplitudes, giving rise to the CBS signal in the weakly inelastic scattering regime. Grey-shaded and black spots represent inelastically and elastically scattering scattering atoms, respectively. The amplitudes spell out the transformation of ingoing frequencies ω_L into outgoing frequencies ω. These interfering amplitudes are non-reciprocal, since the frequencies of the intermediate photons for direct and reversed paths are different.

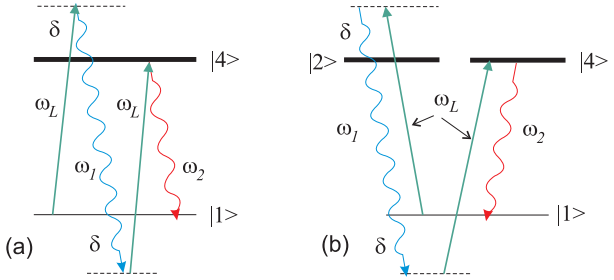

FIG. 5: Two-photon processes describing the laser frequency transformation on the left atom in Fig. 4. (a) corresponds to Fig. 4(a): Two laser photons are converted into two scattered photons such that $\omega_1 \simeq \omega_0 + 2\delta$ and $\omega_2 \simeq \omega_0$. Either one of these photons then travels to the other atom. (b) corresponds to Fig. 4(b) in case $\omega \simeq \omega_1$: One laser photon and one elastically scattered photon give rise to the CBS photon at $\omega \simeq \omega_1$ and the undetected fluorescence photon at $\omega_2 \simeq \omega_0$. The roles of the photons at ω_1 and ω_2 can be interchanged by flipping their polarizations.

final frequencies of the scattered photons are the same, the intermediate frequencies differ, leading to the non-reciprocity of the interfering amplitudes, and a decrease of the CBS enhancement factor. The non-reciprocity argument was also successfully applied to interpret a dispersive resonance of the crossed term's spectrum in the weakly inelastic regime [21].

Figure 4 shows direct (a) and reversed (d) processes contributing to the CBS signal. Without loss of generality, we assume that the left atom is scattering inelastically. The direct, E_1, and reversed, E_2, scattering amplitudes can be derived as [16]

$$E_1 = -\frac{e^{-i\phi/2}(\gamma + i\delta)}{(\gamma + i(\delta - \nu))(\gamma + i(\delta + \nu))^2}, \quad (18)$$

$$E_2 = -\frac{e^{i\phi/2}}{(\gamma + i\delta)^2 + \nu^2}, \quad (19)$$

where ϕ is a phase which depends on the geometric configuration, and should be taken zero in the backscattering direction. From Eqs. (18) and (19), we obtain following expressions for the ladder and crossed spectra:

$$\tilde{L}_2^{\rm inel}(\nu) = \frac{2(\gamma^2 + \delta^2) + 2\delta\nu + \nu^2}{(\gamma^2 + (\delta - \nu)^2)(\gamma^2 + (\delta + \nu)^2)^2}, \quad (20)$$

$$\tilde{C}_2^{\rm inel}(\nu) = \frac{2(\gamma^2 + \delta(\delta + \nu))}{(\gamma^2 + (\delta - \nu)^2)(\gamma^2 + (\delta + \nu)^2)^2}. \quad (21)$$

Expressions (20) and (21) precisely reproduce the spectral lineshape of the ladder and crossed spectra of Fig. 3, and, up to the prefactor $\Omega^4/(8\pi\gamma)$, coincide with the respective results of the master equation approach at vanishing detuning $\delta = 0$ (see Eqs. (B13) and (B14) in Appendix B). They also allow for a transparent interpretation of the CBS spectra for arbitrary detuning δ.

By inspecting the denominators of Eqs. (20) and (21), we see that, at $\delta = 0$, both $\tilde{L}_2^{\rm inel}(\nu)$ and $\tilde{C}_2^{\rm inel}(\nu)$ must exhibit a single peak, at $\nu = 0$, as is the case in Fig. 3(a). At $\delta \neq 0$, there must be two resonances at $\nu \simeq \pm\delta$, with the more pronounced one at $\nu \simeq -\delta$ (since the respective term is squared) (see Fig. 3(b,c)). The physical reason for this behavior is easy to understand by recalling that upon inelastic scattering on the (left, in Fig. 4) atom, the re-emitted photon frequency ω can be either $\omega_L - \delta = \omega_0$ or $\omega_L + \delta = \omega_0 + 2\delta$, as spelled out by the level diagram in Fig. 5. The former, equal to the atomic resonance frequency, corresponds to $\nu \simeq -\delta$, and acquires a large scattering cross-section, while the latter corresponds to $\nu \simeq +\delta$, and has a diminished scattering cross-section since detuned by 2δ from the atomic transition frequency.

Another peculiarity of the CBS spectra which clearly stands out in Fig. 3(c) as well as in Eq. (21) is a dispersive lineshape of the crossed spectrum around $\nu \simeq -\delta$. In other words, as the signal frequency passes from $\omega > \omega_0$ to $\omega < \omega_0$, the interference character between the interference paths (a) and (b) of Fig. 4 turns from constructive to destructive. This is due to the continuous ω-dependence of the phase shift between the direct (18) and reversed (19) scattering amplitudes, passing through $\pi/2$ at $\omega \simeq \omega_0$.

3. *Strongly inelastic scattering*

As the Rabi frequency Ω increases to values $\Omega > \gamma$, scattering processes of higher than second order contribute for the individual atoms, resulting in the emission of the resonance fluorescence Mollow triplet [26]. Correspondingly, the CBS spectra become more complicated at intense driving. Figure 6 presents examples of normalized ladder and crossed spectra for two fixed values of the Rabi frequency, $\Omega = 10\gamma$ (Fig. 6(a-c)), and $\Omega = 20\gamma$ (Fig. 6(d-f)).

At exact resonance, the spectra remain symmetric, with signatures of five resonances at $\nu = \pm\Omega$, $\nu = \pm\Omega/2$,

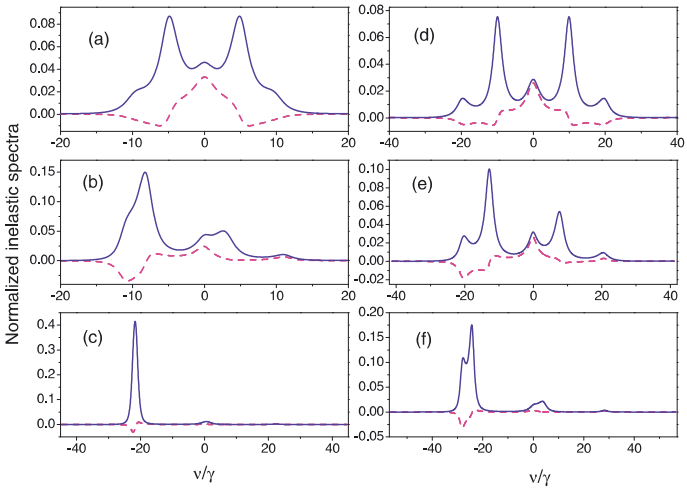

FIG. 6: (Color online) Normalized inelastic spectra of the ladder, $\tilde{L}_2^{\rm inel}$, (solid) and crossed, $\tilde{C}_2^{\rm inel}$, (dashed line) terms. Left panel ((a)-(c)): $\Omega = 10\gamma$; right panel ((d)-(f)): $\Omega = 20\gamma$. The detuning increases from top to bottom: $\delta = 0$ (top); 5γ (middle); 20γ (bottom).

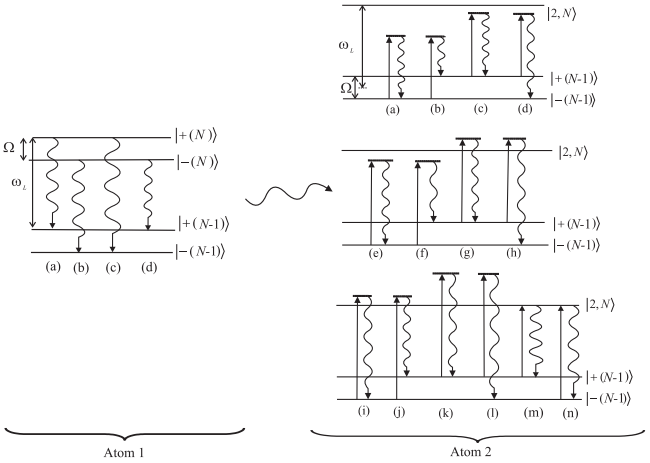

FIG. 7: Single (left) and double (right) scattering processes. Only the laser-driven and the CBS transition are depicted, respectively. Radiative processes (a) and (b) on the left give rise to the Rayleigh peak of the Mollow triplet with linewidth γ centered at $\nu = 0$. (c) and (d) give rise to the sidebands at $\nu = \Omega$ and $\nu = -\Omega$, respectively, with linewidths $3\gamma/2$. Photons emitted by atom 1 (left) propagate to atom 2 (right), and are scattered from either one of the dressed states of the energy manifold with $N-1$ laser photons. The diagrams on the right describe the scattering of: (a)-(d) a sideband photon centered at $\nu = -\Omega$; (e)-(h) a photon from the central peak; (i)-(l) a sideband photon at $\nu = \Omega$; (m), (n) resonant photons at $\nu = \pm\Omega/2$.

and $\nu = 0$. Crossed spectra take negative values in a frequencies range which spares out the central, positive, peak. With increasing δ, some of the resonances approach each other (observe, e. g., the change of position of the two left-most resonances of the ladder term from Fig. 6(a) to (b), and from (d) to (e)), and eventually merge (see Fig. 6(f)). Fig. 6(c) is qualitatively reminiscent of Fig. 3(c), though additionally garnished with a signal at $\nu \simeq 0$ in both the ladder and crossed spectra. This additional resonance stems from the central peak of the Mollow triplet, emerging in three-photon scattering processes on one atom. In contrast, Fig. 3(c) corresponds to a much weaker saturation parameter ($s = 2 \times 10^{-4}$) where three-photon processes are negligible, and hence the central Mollow peak is not visible..

A notable feature of the spectra of Fig. 6 is that, for $\delta = 20\gamma$ ((c) and (f)), the overall inelastic crossed term becomes negative, i.e., $\int_{-\infty}^{\infty} d\nu \tilde{C}_2^{\rm inel}(\nu)/L_2^{\rm inel} = -0.029$ (for $\Omega = 10\gamma$), and -0.066 (for $\Omega = 20\gamma$), respectively. The negative value of the normalized crossed term in the latter case dominates the positive ratio $C_2^{\rm el}/L_2^{\rm inel} = 0.057$ which can be extracted from Fig. 2(c) for $\Omega = 20\gamma$. Therefore, the enhancement factor $\alpha = 1 + (C_2^{\rm el} + C_2^{\rm inel})/(L_2^{\rm el} + L_2^{\rm inel})$ is equal to $0.991 < 1$, in accordance with [20] and Sec. III B 1. It is now clear that the anti-enhancement comes from destructive self-interference of inelastically scattered photons around $\nu = -28\gamma \simeq -\sqrt{\Omega^2 + \delta^2}$, with $\Omega = \delta = 20\gamma$. As seen in Fig. 6(f), at these parameter values, the two resonances at which the crossed spectrum is negative are almost merged. Hence, the destructively interfering processes responsible for each distinct resonance become indistinguishable, and interfere with each other. This interference additionally broadens the negative area of the crossed spectrum, leading to anti-enhancement. As the detuning becomes much larger than the Rabi frequency, only the dispersive resonance of the crossed spectrum survives, leading to a picture qualitatively similar to that of Figs. 3(c), 6(c). The position of this resonance corresponds to the resonance frequency of an ac-Stark shifted CBS transition, and will be specified in the next subsection.

4. *Limit of well-separated spectral lines*

Although the positions of the resonances of the CBS spectrum could be guessed from the results presented in the previous section, the spectral line shape for the ladder and crossed terms is not quite clear, since not yet fully resolved at the Rabi frequency considered. To reach a fully transparent picture, we will now address the limit of well-separated spectral lines, at $\Omega \gg \gamma$.

a. Exact resonance. Let us start with a reminder of the level structure of the pumped (by the driving laser) and probed (by the scattered photon) transitions of both atoms. In an intense laser field with $\Omega \gg \gamma$, the pumped transition $|1\rangle \leftrightarrow |4\rangle$ is strongly coupled to the laser mode. In this case, it is instructive to treat the latter as a quantum system [27, 28]. The eigenstates of the laser-atom interaction Hamiltonian are the dressed states $|\pm(N)\rangle_\alpha$.

For $\delta = 0$, they read

$$|\pm(N)\rangle_\alpha = \frac{1}{\sqrt{2}}(|1, N+1\rangle_\alpha \pm e^{i\mathbf{k}\cdot\mathbf{r}_\alpha}|4, N\rangle_\alpha), \qquad (22)$$

where N and $N+1$ refer to the number of photons in the laser mode, and α labels the atoms. Inasmuch as the dressed states represent superpositions of the ground and *excited* atomic states of the laser-driven transition, they have widths equal to γ for the resonant driving [28]. Spontaneous transitions from the dressed states manifold $\{|\pm(N)\rangle_\alpha\}$ to $\{|\pm(N-1)\rangle_\alpha\}$ lead to emission of the fluorescence spectrum centered at frequencies $\omega_L - \Omega$, ω_L, and $\omega_L + \Omega$ known as the Mollow triplet [26] (see the left of Fig. 7). The width of the central peak is defined by the decay rate of the dressed state's populations, and is equal to 2γ, while the width of the sidebands is determined by the decay rate of the coherences between the dressed states, and is equal to 3γ [28].

On the other hand, the level $|2\rangle$ is not affected by the laser field. As a result, the probed transition $|1\rangle \leftrightarrow |2\rangle$ of both atoms, giving rise to CBS photons, is affected by the laser field only via the state $|1\rangle$. For that reason, new resonance frequencies of the probed transition emerge at $\omega_L \pm \Omega/2$ (the right of Fig. 7).

When the Mollow triplet emitted by one atom is incident on another atom, it is scattered on the internal structure of the latter. Relevant scattering processes that can take place are depicted on the right of Fig. 7. Each photon can be scattered either elastically or undergo Raman-Stokes or -anti-Stokes (multiphoton) transitions [29] (which lead to a frequency change by $-\Omega$ or Ω, respectively), which conserve energy and angular momentum. It follows that the CBS spectrum must have resonances at $\nu = \pm 2\Omega$, $\nu = \pm\Omega$, and $\nu = 0$. The diagramms describing the emission of CBS photons at these frequencies are (a)-(l) on the right of Fig. 7.

However, there are two more diagrams, (m) and (n), that apparently do not fit into the scheme just described. On these diagrams, photons with frequencies $\nu = \pm\Omega/2$ are resonantly scattered to give rise to an additional doublet in the CBS spectrum. This is nothing but an Autler-Townes doublet [30, 31]: One should bear in mind that a Lorentzian distribution has long tails, and thus emission of photons with frequencies very different from the central frequencies is not impossible, though with very small probabilities. For instance, two laser photons may be transformed into two fluorescence photons with frequencies $\omega_L + \Omega/2$ and $\omega_L - \Omega/2$, with each of these photons appearing as a result of quantum interference between the Rayleigh and Raman-anti-Stokes or -Stokes transitions, respectively [32].

What makes the frequencies $\omega_L \pm \Omega/2$ special in our present problem is that both (dressed) atoms have two transitions *exactly in resonance* with these frequencies. Therefore, although the probability of the creation of a pair of photons with frequencies $\omega_L \pm \Omega/2$ is relatively small, the probability of their *double* scattering is high, due to a large resonant scattering cross-section on the transition $|1\rangle \leftrightarrow |2\rangle$ modified by the ac-Stark effect. The overall effect finally acquires the same strength as the elastic (though non-resonant) scattering of photons which are emitted into the dominant frequency components of the Mollow triplet, by the first atom.

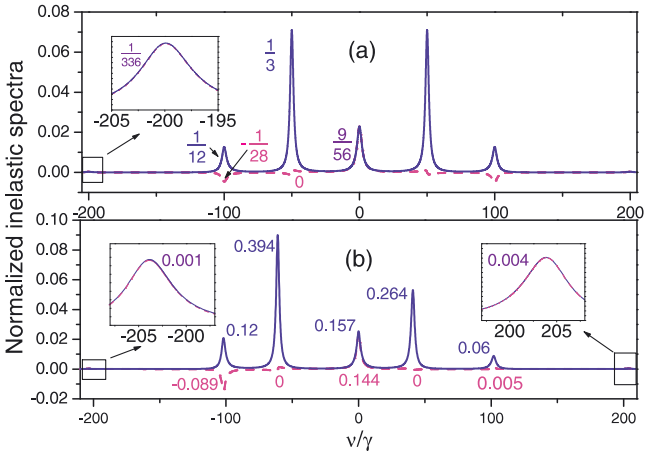

FIG. 8: (Color online) Normalized inelastic spectra of the ladder, $\tilde{L}_2^{\rm inel}(\nu)$ (solid), and crossed, $\tilde{C}_2^{\rm inel}$ (dashed), terms, in the limit of well separated spectral lines, at $\Omega = 100\gamma$. $\delta =$ (a) 0; (b) 20γ. The numbers near the resonances indicate their areas, such that the overall areas of the ladder and crossed terms give unity and $C_2^{\rm inel}/L_2^{\rm inel}$, respectively.

The results of our calculation are presented in Fig. 8(a). Consistently with our analysis, both the ladder and crossed spectra consist of seven resonances, with the positions precisely at the predicted frequencies, that is, at $\nu = \pm 2\Omega$, $\nu = \pm\Omega$, $\nu = \pm\Omega/2$, $\nu = 0$. The respective analytic expressions, (B19) and (B20), can be found in Appendix B.

Let us now discuss the ladder spectrum in more detail, while postponing the analysis of the spectrum of the interference contribution for the next subsection. In the ladder spectrum, three of its resonances, at $\nu = 0$ and $\nu = \pm\Omega$, represent sums of two Lorentzians with different widths. The remaining ones are simple Lorentzians. In order to understand this structure quantitatively, let us reinspect the diagrams on the right of Fig. 7: We start with the central CBS resonance at $\nu = 0$. Several processes, (d), (e), (g), and (j) on the right of Fig. 7 contribute. Diagrams (e) and (g) represent a photon emitted by the first atom into the inelastic Rayleigh component (centered at ω_L), elastically scattered on the dressed states $|+(N-1)\rangle$ and $|-(N-1)\rangle$. The corresponding amplitudes add coherently, so that the two scattering processes are equivalent to elastic scattering by the atomic ground state $|1\rangle$. Since the ground state does not have a linewidth, the resulting frequency distribution is the same as for the Rayleigh component of the resonance fluorescence spectrum, that is, the width 2γ of the excited atomic levels. In contrast, the processes (d) and (j) involve sideband photons centered at either $\omega_L + \Omega$ or $\omega_L - \Omega$ undergo Raman process on $|+(N-1)\rangle$ or

$|-(N-1)\rangle$, respectively. This leads to an additional broadening of the frequency distribution of photons, associated with these transitions, by 3γ. Neither of the processes (d) and (j) interferes with (e) and (g), because the frequency changes associated with these transitions are different, and information about the latter is carried into the environment by the undetected photons [16]. As a result, each of the processes (d) and (j) contributes to the CBS ladder spectrum with a Lorentzian centered at $\nu = 0$, with linewidth 6γ, which adds to the one due to the Rayleigh transitions.

As for the sidebands at $\nu = \pm\Omega$, there are three processes contributing to each of them. Since the spectrum is symmetric, let us analyse the low-frequency sideband. The relevant processes are (a), (c), and (f) in Fig. 7. Processes (a) and (c) are completely analogous to (e) and (g). That is, they add coherently, and the resulting linewidth is the same as for sideband photons of the single-atom spectrum, that is, 3γ. The process (f) is analogous to the process (j), hence the linewidth of the respective Lorentzian must be the sum of the linewidths of the Rayleigh photon and of a dressed state. Thus, we obtain a Lorentzian with linewidth 5γ centered at $\omega_L - \Omega$.

We proceed in the same manner with the sidebands at $\nu = \pm 2\Omega$. The respective diagrams for the lower-frequency sideband are (b) and (l). Since, in both cases, the sideband photons of the resonance fluorescence spectrum undergo Raman processes, the linewidth of the associated Lorentzian is 6γ.

Also note that the crossed term has the same lineshape as the ladder term, at $\nu = \pm 2\Omega$ [see Fig. 8(a)]. This peculiarity of the CBS spectrum will be discussed in more detail in the next subsection. In brief, it is related to the fact that there is only one direct and its reciprocal process, which contribute to the CBS spectral lines at either one of these frequencies. Therefore, these inelastic photons (self-)interfere perfectly well. Although the contribution of the processes at $\nu = \pm 2\Omega$ is very small, it is non-negligible. The numbers for the integral contributions of the ladder and crossed terms to the resonances in Fig. 8(a) (these numbers can be easily extracted from Eqs. (B19) and (B20)) yield precisely the asymptotic value of the enhancement factor $\alpha_\infty = 23/21$ derived in [20]. Without the contributions from the outer sidebands, one would underestimate α_∞ by approximately 6%.

Finally, let us consider the doublet at $\omega_L \pm \Omega/2$. The respective diagrams in Fig. 7, (m) and (n), describe the resonant scattering of photons on the transitions $|+(N-1)\rangle \to |2\rangle$ and $|-(N-1)\rangle \to |2\rangle$. Since the incoming photons do not originate from the (Mollow) peaks of the resonance fluorescence spectrum emitted by the first atom, the corresponding linewidths are only defined by the linewidths of the 'filtering' transitions of the second atom. These linewidths 3γ are a sum of the width 2γ of the excited level $|2\rangle$, and the linewidth γ of either of the dressed states.

b. Detuned case. For $\delta \neq 0$, the major part of the above analysis for $\delta = 0$ is still valid. Though some modifications are needed, in order to explain why some resonances creep towards the other ones; their weights are redistributed, and even the interference character of some of them is changed (see Fig. 8(b)). Here, we will comment on their linewidths and positions.

To derive the new linewidths of the ladder term, one needs to account for the dependence of linewidths of the resonance fluorescence spectrum of the first atom on the detuning [26]. With that and Fig. 7, one easily obtains the linewidths of the CBS ladder spectrum, at finite δ.

It is easy to show that the new resonance frequencies of the CBS transition $|1\rangle \leftrightarrow |2\rangle$, modified by the ac-Stark effect, are $\omega_0 \pm (\Omega' \pm \delta)/2$, where $\Omega' = \sqrt{\Omega^2 + \delta^2}$ is the modified Rabi frequency [26]. It follows that for the detuned case, seven CBS resonances manifest at $\nu = \pm 2\Omega'$ $\nu = \pm\Omega'$, $\nu = \pm(\Omega' \mp \delta)/2$, and $\nu = 0$. Therefore, as we increase the detuning, the Autler-Townes doublet centered at $\nu = -(\Omega' + \delta)/2$ approaches the sideband at $\nu = -\Omega'$, whereas its counterpart centered at $\nu = (\Omega' - \delta)/2$ approaches the central resonance, as evident from Fig. 8(b).

Since the single-atom resonance fluorescence spectrum is always symmetric, this also explains why the sideband at $\nu = -\Omega'$ which is red-shifted with respect to $\nu = 0$ gains more weight than its blue-shifted counterpart: It is closer to the transition frequency $\omega_0' = \omega_0 - (\Omega' - \delta)/2$ as compared to the distance of the sideband at $\nu = \Omega'$ from $\omega_0'' = \omega_0 + (\Omega' - \delta)/2$. Consequently, the associated scattering cross-section is larger. This also explains a larger value of the peak at $\nu = -(\Omega' + \delta)/2$ than at $\nu = (\Omega' - \delta)/2$, given that, under the detuned driving, these resonances originate mainly from the two sidebands of the Mollow triplet. However, when we consider Raman scattering at $\nu = \pm 2\Omega'$, the scattering cross-section for a photon at $\omega_L + \Omega'$ depends on its detuning $(\Omega' + \delta)/2$ from the transition $|2, N\rangle \leftrightarrow |+(N-1)\rangle$ [see Fig. 7(l)]. Likewise, the cross-section for a photon at $\omega_L - \Omega'$ is determined by its detuning $(3\Omega' - \delta)/2$ from the transition $|2, N\rangle \leftrightarrow |-(N-1)\rangle$ [see diagram (b) on the right of Fig. 7]. For $\Omega = 100\gamma$ and $\delta = 20\gamma$, the latter detuning is obviously larger, leading to a redistribution of signal weights in favor of the blue-shifted sideband [compare the insets of Fig. 8(b)]. Note also that this asymmetry does not spoil the perfectness of the interference of CBS photons around $\nu = \pm 2\Omega'$.

C. Interpretation of the crossed spectrum at $\delta = 0$

Finally, for an intuitive interpretation of the interference character of different components of the crossed term's spectrum, we will rely upon the diagrammatic technique developed in [16]. We will see that a slightly modified version thereof in terms of dressed states allows for the explanation of the destructive interference at $\nu = \pm\Omega$, of the dispersive resonances at $\nu = \pm\Omega/2$,

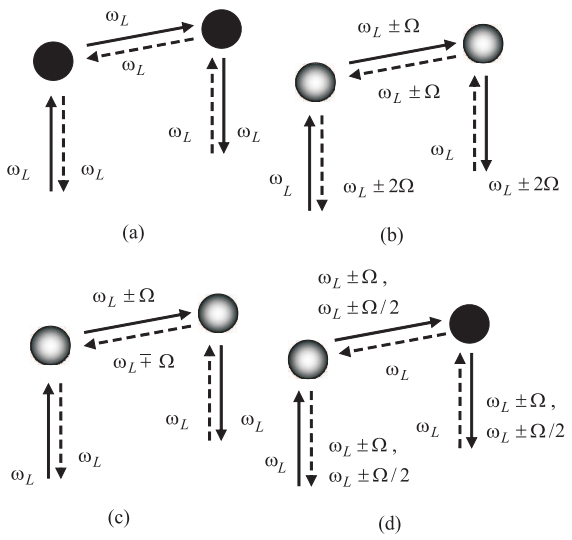

FIG. 9: Qualitative interpretation of the interference character. Grey-shaded and black spots represent atoms scattering inelastically and quasi-elastically, respectively. Solid and dashed arrows correspond to direct and reversed scattering amplitudes, respectively. In examples (a) and (b), the direct and the reversed amplitudes are reciprocal, whereas they are not in cases (c) and (d).

and of the constructive interferences at the other resonances.

Let us first note that the interference character of different resonances of the crossed spectrum is defined by how much, if at all, the outgoing light frequency is shifted with respect to the incoming laser frequency ω_L. In the secular limit $\Omega \gg \gamma$, these shifts are of the order of Ω, with the widths of the shifts' distribution of the order of γ. Frequency shifts give rise to phase shifts between the interfering amplitudes. Taking into account the continuous ω-dependence of the amplitudes' phases, we will ignore the frequency changes of the order of γ, and refer to the respective scattering processes as 'quasi-elastic'. We will label 'inelastic' the processes upon which the frequency changes by the quantity of the order of Ω.

With these preliminaries, we will use diagrams similar to that of Fig. 4, to depict direct and reversed scattering amplitudes for the scattering processes contributing to the CBS spectrum, in the limit of well-separated spectral lines (see Fig. 8). These diagrams, shown in Fig. 9, split into three categories: (a), both atoms scatter quasi-elastically; (b), (d), both atoms scatter inelastically; (c), one of the two atoms scatters inelastically. When both atoms scatter quasi-elastically [Fig. 9(a)], or inelastically – into the outer sidebands [Fig. 9(b)], there is a reciprocal, reversed process, such that the interference is perfect, as indeed observed for peaks at $\nu \simeq 0$ and $\nu \simeq \pm 2\Omega$ of Fig. 8(a), since there, the crossed and the ladder contributions are indistinguishable. However, note that, since each inelastic event induces the same change of frequency for both reversed processes, the intermediate photons ($\omega_L \pm \Omega$) have opposite detuning from the laser frequency in Fig. 9(c). In the case $\delta = 0$, those two frequencies are equally far detuned from the atomic resonance, and, as evident from Fig. 8(a), the equality between the reversed amplitudes remains preserved. Only for non-vanishing detuning, the interference contrast at $\nu = 0$ is slightly reduced, see Fig. 8(b), where the weights of the crossed and ladder contribution (0.144 and 0.157) are different.

Now let us address diagram (d) of Fig. 9 which is reminiscent of Fig. 4. This diagram shows non-reciprocal interfering amplitudes, which, depending on the frequency shifts between the intermediate photons for direct and reversed paths, can describe either the dispersive features (which corresponds to $\nu = \pm\Omega/2$) of the crossed term's spectrum, or the destructive interference thereof (at $\nu = \pm\Omega$). In order to see this, we will construct explicit expressions for the direct and reversed scattering amplitudes. Although both atoms are driven by a powerful laser field, it is sufficient to consider the *two-photon* scattering amplitudes, as in Fig. 4, provided that the ac-Stark shifts of the CBS transition $|2\rangle \leftrightarrow |1\rangle$ as well as of the laser-driven transition $|4\rangle \leftrightarrow |1\rangle$ are properly accounted for. In other words, for the CBS transition, instead of considering the atomic resonance frequency ω_0, one should consider two resonance frequencies $\omega_0' = \omega_0 - \Omega/2$ and $\omega_0'' = \omega_0 + \Omega/2$. On the other hand, ω_0 remains the resonance frequency for the laser-driven transition. It should be stressed that our present treatment is very schematic and does not pretend to be a full explanation of the interference character in the saturation regime. Rather, we aim here at a qualitative understanding of the interference effect as observed in Fig. 8.

In order to construct the direct and reversed amplitudes, E_1 and E_2, respectively, we employ the symmetry of the CBS spectrum at $\delta = 0$ with respect to a change of the sign of ν, and consider only the interference character of the two resonances, at $\nu_* \simeq \Omega, \Omega/2$. In the direct two-photon process, photons with frequencies $\omega_L + \nu_*$ and $\omega_L - \nu_*$ are scattered by the first atom. We assume that the detected photon with frequency $\omega_* = \omega_L + \nu_*$ is quasi-elastically scattered on an ac-Stark shifted transition with frequency ω_0'' of the second atom, since ω_* is closer to the modified transition frequency ω_0'' than to the one with frequency ω_0'. For the reversed amplitude, a laser photon is scattered quasi-elastically by the second atom. Then, the first atom scatters inelastically a pair of photons with frequency ω_L into photons with frequencies ω_* and $2\omega_L - \omega_*$, with the detected photon originating from the Raman-anti-Stokes scattering on the ac-Stark shifted transition with the resonance frequency ω_0', while the undetected photon scatters on the laser-driven transition, for which ω_0 is the resonance frequency.

With the above assumptions, the amplitudes E_1 and

E_2 read

$$E_1 = \Big(\frac{1}{\nu_* - i\gamma} - \frac{1}{\nu_* + i\gamma}\Big)\frac{e^{-i\phi/2}}{\nu_* - \Omega/2 - i\gamma}, \quad (23)$$

$$E_2 = \Big(\frac{1}{\nu_* + \Omega/2 - i\gamma} - \frac{1}{\nu_* + i\gamma}\Big)\frac{ie^{i\phi/2}}{\gamma}. \quad (24)$$

It is easy to check that the phase shift between the non-reciprocal amplitudes (23) and (24) continuously depends on ω_* (or ν_*). For $\nu_* \simeq \Omega/2$, in full analogy with the case studied in Sec. III B 2 [since ν_* corresponds to the (modified) transition frequency], the interfering amplitudes are phase shifted by approximately $\pi/2$, and thus describe a dispersive line shape, under slight variation of ν_*. The same amplitudes, for $\nu_* \simeq \Omega$, are phase shifted by approximately π and therefore interfere destructively. This is quite analogous to the interference-induced anti-enhancement of CBS in the regime of elastic scattering, due to the non-reciprocity of combined Rayleigh and Raman scattering processes [33]. Both the dispersive line shape and the anti-enhancement is precisely what is observed in Fig. 8(a).

IV. CONCLUSION

We presented a detailed calculation of the spectrum of coherent backscattering of light by two identical, randomly placed atoms, for arbitrary strengths of the laser field.

We saw that the CBS spectrum exhibits its most complicated structure in the limit of strong driving. The ladder term's spectrum reveals seven Lorentzian peaks which represent: (i) Mollow triplet photons (re-)scattered by the second atom, with resonances at $\omega = \omega_L - \Omega$, $\omega = \omega_L$, $\omega = \omega_L + \Omega$; (ii) an Autler-Townes doublet with resonances at $\omega = \omega_L - \Omega/2$ and $\omega = \omega_L + \Omega/2$; (iii) a doublet originating from the Raman Stokes scattering of the low-frequency sideband, and from the Raman anti-Stokes scattering of the high-frequency sideband of the Mollow triplet, with resonance frequencies $\omega = \omega_L - 2\Omega$ and $\omega = \omega_L + 2\Omega$, respectively.

The crossed term's spectrum reveals resonances located at the same frequencies as those of the ladder term. We interpreted the interference character of different resonances through reciprocity arguments applied to dressed states. Interference is always constructive for the central resonance at $\omega = \omega_L$, and for the outer sidebands at $\omega = \pm 2\Omega$. It changes character in the vicinity of the Autler-Townes doublet (at $\omega = \omega_L \pm \Omega/2$, where the crossed term's spectrum is described by a dispersive curve), and contributes a negative Lorentzian at $\omega = \omega_L \pm \Omega$.

For the case of the detuned driving, at $|\delta| \simeq \Omega$, one of the dispersive resonances overlaps with one of the negative Lorentzians. Interference between the scattering processes responsible for appearance of these two resonances may lead to CBS anti-enhancement.

Acknowledgments

Useful discussions with Dominique Delande, Sergei Kilin, Dmitry Kupriyanov, Christian Miniatura, Cord Müller, Alexander Nizovtsev, Marlan Scully, Igor Sokolov, and Carlos Viviescas are gratefully acknowledged.

APPENDIX A: CBS INTENSITY AND ENHANCEMENT FACTOR

1. Derivation procedure

The operator master equation (5) leads to the linear matrix equation

$$\langle\dot{\mathbf{Q}}\rangle = (\mathbf{A} + \mathbf{V})\langle\mathbf{Q}\rangle + \mathbf{j}. \quad (A1)$$

Here, vector $\mathbf{Q}$ having 255 elements is obtained from the tensor product $\mathbf{q}_1 \otimes \mathbf{q}_2$, where

$$\mathbf{q} = (\mathbb{1}/2, \mu_1/2, \mu_2/2, \mu_3/2, \sigma_{14}, \sigma_{41}, \sigma_{13}, \sigma_{31}, \sigma_{12}, \sigma_{21}, \sigma_{34}, \sigma_{43}, \sigma_{42}, \sigma_{24}, \sigma_{32}, \sigma_{23})^T \quad (A2)$$

is a vector whose elements comprise the complete orthonormal basis set of operators for a four-level quantum system, and indices '1' and '2' number atoms. In Eq. (A2),

$$\mathbb{1} = \sigma_{11} + \sigma_{22} + \sigma_{33} + \sigma_{44}, \quad (A3a)$$

$$\mu_1 = \sigma_{22} - \sigma_{33} + \sigma_{44} - \sigma_{11}, \quad (A3b)$$

$$\mu_2 = \sigma_{22} - \sigma_{33} - \sigma_{44} + \sigma_{11}, \quad (A3c)$$

$$\mu_3 = \sigma_{22} + \sigma_{33} - \sigma_{44} - \sigma_{11}. \quad (A3d)$$

In order to describe a mapping of the elements of the two 16×16 vectors onto the vector with 255 elements, it is convenient to numerate the basis operators starting from '0'. We will denote the ith element of a vector $\mathbf{a}$ by $[\mathbf{a}]_i$. For instance, $[\mathbf{q}_1]_0 = \mathbb{1}_1/2$. With these rules, we map element $\langle[\mathbf{q}_1]_l \otimes [\mathbf{q}_2]_m\rangle$ onto $\langle[\mathbf{Q}]_n\rangle$, where $n = 16l + m$, $0 \le l, m \le 15$. After we exclude the first element of the tensor product (it corresponds to $l = m = 0$), we obtain that n runs from 1 to 255. Then, the matrices $\mathbf{A}$, $\mathbf{V}$, and $\mathbf{j}$ are generated by inserting 255 elements of the vector $\mathbf{Q}$ to Eqs. (6), (7) and performing the quantum mechanical averaging:

$$\langle(\mathcal{L}_\alpha + \mathcal{L}_\beta)[\mathbf{Q}]_n\rangle = \sum_{m=1}^{255} A_{nm}\langle[\mathbf{Q}]_m\rangle + [\mathbf{j}]_n, \quad (A4a)$$

$$\langle(\mathcal{L}_{\alpha\beta} + \mathcal{L}_{\beta\alpha})[\mathbf{Q}]_n\rangle = \sum_{m=1}^{255} V_{nm}\langle[\mathbf{Q}]_m\rangle. \quad (A4b)$$

From the Laplace transform solution to Eq. (A1), $\langle\tilde{\mathbf{Q}}(z)\rangle = (z\mathbb{1}_{255} - \mathbf{A} - \mathbf{V})^{-1}(\langle\mathbf{Q}(0)\rangle + z^{-1}\mathbf{j})$, where z is defined in the main text after Eq. (4), and $\mathbb{1}_{255}$ is the

unit 255×255 matrix, we extract the steady state solution $\langle \mathbf{Q} \rangle_{\rm ss} = \lim_{z\to 0} z\langle \tilde{\mathbf{Q}}(z)\rangle$.

The double scattering contribution corresponds to the perturbative expansion of $\langle \mathbf{Q} \rangle_{\rm ss}$ to the second order in the coupling constant g, $\langle \mathbf{Q} \rangle_{\rm ss}^{[2]} = \mathbf{G}_0\mathbf{V}\mathbf{G}_0\mathbf{V}\mathbf{G}_0\mathbf{j}$, where $\mathbf{G}_0 \equiv -\mathbf{A}^{-1}$. Finally, the correlation functions relevant for the evaluation of the total ladder and crossed contributions [see Eqs. (11), (12)] read

$$\langle \sigma_{21}^1\sigma_{12}^2\rangle_{\rm ss}^{[2]} = \langle [\mathbf{Q}]_{152}\rangle_{\rm ss}^{[2]}, \tag{A5a}$$
$$\langle \sigma_{12}^1\sigma_{21}^2\rangle_{\rm ss}^{[2]} = \langle [\mathbf{Q}]_{137}\rangle_{\rm ss}^{[2]}, \tag{A5b}$$
$$2\langle \sigma_{22}^1\rangle_{\rm ss}^{[2]} = \langle [\mathbf{Q}]_{16}\rangle_{\rm ss}^{[2]} + \langle [\mathbf{Q}]_{32}\rangle_{\rm ss}^{[2]} + \langle [\mathbf{Q}]_{48}\rangle_{\rm ss}^{[2]}, \tag{A5c}$$
$$2\langle \sigma_{22}^2\rangle_{\rm ss}^{[2]} = \langle [\mathbf{Q}]_{1}\rangle_{\rm ss}^{[2]} + \langle [\mathbf{Q}]_{2}\rangle_{\rm ss}^{[2]} + \langle [\mathbf{Q}]_{3}\rangle_{\rm ss}^{[2]}. \tag{A5d}$$

Concerning the elastic ladder and crossed terms [see Eq. (15)], the relevant dipole moment expectation values are given by

$$\langle \sigma_{12}^1\rangle_{\rm ss}^{[1]} = \langle [\mathbf{Q}]_{128}\rangle_{\rm ss}^{[1]},\ \langle \sigma_{21}^1\rangle_{\rm ss}^{[1]} = \langle [\mathbf{Q}]_{144}\rangle_{\rm ss}^{[1]}, \tag{A6a}$$
$$\langle \sigma_{12}^2\rangle_{\rm ss}^{[1]} = \langle [\mathbf{Q}]_{8}\rangle_{\rm ss}^{[1]},\quad \langle \sigma_{21}^2\rangle_{\rm ss}^{[1]} = \langle [\mathbf{Q}]_{9}\rangle_{\rm ss}^{[1]}, \tag{A6b}$$

where $\langle \mathbf{Q} \rangle_{\rm ss}^{[1]} = \mathbf{G}_0\mathbf{V}\mathbf{G}_0\mathbf{j}$.

Numerical results for the elastic and inelastic intensities for different detunings can be found in the main text. In the next subsection, we will present analytical results for the case of exact resonance.

2. Analytical results for $\delta = 0$

Evaluating correlation functions from Eq. (A5), we arrive at following results [20]

$$2\,\mathrm{Re}\,\{\langle \sigma_{21}^1\sigma_{12}^2\rangle_{\rm ss}^{[2]} e^{i\mathbf{k}\cdot\mathbf{r}_{12}}\} = |g|^2 |\overleftrightarrow{\mathbf{\Delta}}_{+1,+1}|^2 \frac{R_1(s)}{(4+s)P(s)} \times \cos\{(\mathbf{k}+\mathbf{k}_L)\cdot\mathbf{r}_{12}\}, \tag{A7}$$
$$\langle \sigma_{22}^1\rangle_{\rm ss}^{[2]} + \langle \sigma_{22}^2\rangle_{\rm ss}^{[2]} = |g|^2 |\overleftrightarrow{\mathbf{\Delta}}_{+1,+1}|^2 \frac{R_2(s)}{P(s)}. \tag{A8}$$

$R_1(s)$, $R_2(s)$, and $P(s)$ are polynomial expressions in the on-resonance saturation parameter $s = \Omega^2/2\gamma^2$,

$$R_1(s) = \frac{2}{9}\left(6912s + 3168s^2 + 264s^3 + 20s^4 + s^5\right), \tag{A9a}$$
$$R_2(s) = \frac{1}{3}\left(1152s + 528s^2 + 132s^3 + 7s^4\right), \tag{A9b}$$
$$P(s) = (1+s)^2(12+s)(32+20s+s^2), \tag{A9c}$$

and $\overleftrightarrow{\mathbf{\Delta}}_{+1,+1} = \hat{\mathbf{e}}_{+1}\cdot\overleftrightarrow{\mathbf{\Delta}}\cdot\hat{\mathbf{e}}_{+1}$.

The configuration average of (A7) and (A8) leads to the final result

$$C_2^{\rm tot}(\theta) \simeq \frac{|\bar{g}|^2 R_1(s)}{(4+s)P(s)}\Big(\frac{2}{15} - \frac{(k\,\ell\,\theta)^2}{35}\Big), \tag{A10}$$
$$L_2^{\rm tot} = \frac{2|\bar{g}|^2 R_2(s)}{15P(s)}, \tag{A11}$$

with $\bar{g} = g|_{r_{\alpha\beta}=\ell}$. The scattering angle $\theta = 2\arcsin\{|\mathbf{k}+\mathbf{k}_L|/2k_L\} \ll 1$ with respect to the backscattering direction was assumed to be sufficiently small herein.

The enhancement factor $\alpha(s)$, Eq. (13), deduced from Eqs. (A10) and (A11) reads

$$\alpha(s) = 1 + \frac{R_1(s)}{(4+s)R_2(s)}, \tag{A12}$$

and $\alpha(0) = 2.0$ in the weak field limit, as it must be in the elastic scattering regime. For small s, enhancement linearly decreases as $2 - s/4$, in full agreement with the diagrammatic theoretical result [16] and in qualitative agreement with the result of Sr experiment [8]. When s increases further, α monotonically drops to an asymptotic value $\lim_{s\to\infty}\alpha(s) = \alpha_\infty = 23/21$ [20] which is strictly larger than unity, implying a residual constructive interference in the deep saturation regime.

We will next show that this interference is due to inelastic photons only. Indeed, we obtained the following result for the elastic ladder and crossed terms

$$L_2^{\rm el} = C_2^{\rm el} = \frac{2|\bar{g}|^2}{15}\frac{s}{(1+s)^4}. \tag{A13}$$

As seen from Eq. (A13) the elastic component shows perfect contrast for all s. In particular, it is this component that results in enhancement $\alpha = 2$ for very small $s \to 0$. However, in the deep saturation regime, this component decreases as s^{-3}, while the counterparts of the total intensity, Eqs. (A10), (A11), as s^{-1}. Herefrom follows our conclusion about the origin of the residual enhancement in the deep saturation regime. Explicitly, the inelastic crossed and ladder terms obtained by elementary substraction of Eq. (A13) from Eqs. (A10) and (A11) read

$$C_2^{\rm inel} = \frac{2|\bar{g}|^2}{15}\frac{20736s^2 + \ldots + 2s^7}{9(1+s)^2(4+s)P(s)}, \tag{A14}$$
$$L_2^{\rm inel} = \frac{2|\bar{g}|^2}{15}\frac{2016s^2 + \ldots + 7s^6}{3(1+s)^2P(s)}, \tag{A15}$$

where we have retained only the lowest and highest order terms in the numerators, because these terms will be used to verify the expressions for the spectra. Explicit values of other coefficients are not important. Using (A14) and (A15), it is easy to verify that $\lim_{s\to\infty} C_2^{\rm inel}/L_2^{\rm inel} = 2/21 = \alpha_\infty - 1$.

APPENDIX B: DERIVATION OF CBS SPECTRUM FROM EQ. (5)

1. Elastic and inelastic spectra

By virtue of the quantum regression theorem [24], the temporal correlation functions of a Markov process obey the same equation of motion as the expectation values of operators, that is, Eq. (5), but with different initial conditions and a different free term. The latter can be

straightforwardly determined provided that the stationary solution to Eq. (5) is known.

The four correlation functions appearing in the definition of the spectrum [see Eqs. (3), (4)] can be extracted from the following correlation functions:

$$\mathbf{s}_\alpha(t) \equiv \langle \sigma_{21}^\alpha \mathbf{Q}(t)\rangle_{\rm ss} \quad (\alpha = 1, 2), \tag{B1}$$

where $\mathbf{s}_\alpha(t)$ is a vector containing, like $\langle \mathbf{Q}(t)\rangle$, 255 elements. The vector $\mathbf{s}_\alpha(t)$ satisfies the equation of motion

$$\dot{\mathbf{s}}_\alpha = (\mathbf{A} + \mathbf{V})\mathbf{s}_\alpha + \langle \sigma_{21}^\alpha \rangle_{\rm ss} \mathbf{j}, \tag{B2}$$

which explicitly accounts for the modification of the free term. From the definition (B1), it follows that the vectors $\mathbf{s}_1$ and $\mathbf{s}_2$ are obtained from $\langle \mathbf{q}_1' \otimes \mathbf{q}_2\rangle_{\rm ss}$ and $\langle \mathbf{q}_1 \otimes \mathbf{q}_2'\rangle_{\rm ss}$, respectively, where

$$\begin{aligned} \mathbf{q}' \;=\; & (\sigma_{21}/2, -\sigma_{21}/2, \sigma_{21}/2, -\sigma_{21}/2, \sigma_{24}, 0, \sigma_{23}, 0, \\ & \sigma_{22}, 0, 0, 0, 0, 0, 0, 0)^T, \end{aligned} \tag{B3}$$

by using the same mapping rule as described previously in Sec. A 1. Finally, to find the initial conditions for these vectors, one just needs to make certain transpositions among the elements of the vector $\langle \mathbf{Q}\rangle_{\rm ss}$.

The Laplace transform solution of Eq. (B2) reads:

$$\tilde{\mathbf{s}}_\alpha(z) = \frac{1}{z\mathbb{1}_{255} - (\mathbf{A} + \mathbf{V})}\Big[\mathbf{s}_\alpha(0) + \frac{\mathbf{j}}{z}\langle \sigma_{21}^\alpha \rangle_{\rm ss}\Big], \tag{B4}$$

where $\tilde{\mathbf{s}}_\alpha(z)$ is a Laplace image of $\mathbf{s}_\alpha(t)$. Using this solution and definitions

$$\langle \sigma_{12}^1\rangle_{\rm ss} = 2\langle [\mathbf{q}_1]_8 \otimes [\mathbf{q}_2]_0\rangle, \;\; \langle \sigma_{12}^2\rangle_{\rm ss} = 2\langle [\mathbf{q}_1]_0 \otimes [\mathbf{q}_2]_8\rangle, \tag{B5}$$

we arrive at the following expression for the Laplace image of the correlation function

$$\begin{aligned} \tilde{G}_{\rm ss}^{(1)}(z) \;=\; & 2([\tilde{\mathbf{s}}_1(z)]_{128} + [\tilde{\mathbf{s}}_2(z)]_8 \\ & + [\tilde{\mathbf{s}}_1(z)]_8 e^{i\mathbf{k}\cdot\mathbf{r}_{12}} + [\tilde{\mathbf{s}}_2(z)]_{128} e^{-i\mathbf{k}\cdot\mathbf{r}_{12}}), \end{aligned} \tag{B6}$$

The next step will be to extract the lowest-order in the coupling g, nonvanishing contribution from (B4) and insert it into Eq. (B6). This contribution is on the order g^2 and corresponds to double scattering in which the atoms exchange a photon. Explicitly,

$$\begin{aligned} \tilde{\mathbf{s}}_\alpha^{[2]}(z) \;=\; & \mathbf{G}_0(z)\mathbf{V}\mathbf{G}_0(z)\mathbf{V}\mathbf{G}_0(z)\Big[\mathbf{s}_\alpha^{[0]}(0) + \frac{\mathbf{j}}{z}\langle \sigma_{21}^\alpha \rangle_{\rm ss}^{[0]}\Big] \\ & + \mathbf{G}_0(z)\mathbf{V}\mathbf{G}_0(z)\Big[\mathbf{s}_\alpha^{[1]}(0) + \frac{\mathbf{j}}{z}\langle \sigma_{21}^\alpha \rangle_{\rm ss}^{[1]}\Big] \\ & + \mathbf{G}_0(z)\Big[\mathbf{s}_\alpha^{[2]}(0) + \frac{\mathbf{j}}{z}\langle \sigma_{21}^\alpha \rangle_{\rm ss}^{[2]}\Big], \end{aligned} \tag{B7}$$

where $\mathbf{G}_0(z) = (z\mathbb{1}_{255} - \mathbf{A})^{-1}$, and the superscripts [0], [1], and [2] indicate terms on the order g^0, g^1, and g^2, respectively.

Expression (B7) can be simplified since (B6) gives a spectrum in the $h \parallel h$ channel. Therefore, the stationary expectation values of operators related to the laser-nondriven transition vanish in g^0. So, the first, second, and last terms must be dropped from (B7). Concerning the latter term, it does not contribute to (B6) since $[\mathbf{G}_0(z)\mathbf{j}]_8$ and $[\mathbf{G}_0(z)\mathbf{j}]_{128}$ give $\langle \sigma_{12}^2\rangle_{\rm ss}^{[0]}$ and $\langle \sigma_{12}^1\rangle_{\rm ss}^{[0]}$, respectively, and thus vanish for the reason already indicated.

It is useful to split the nonvanishing part of (B7) into two counterparts from which the elastic and inelastic spectra are extracted:

$$\tilde{\mathbf{s}}_\alpha^{[2]}(z) = \tilde{\mathbf{s}}_{\alpha;{\rm el}}^{[2]}(z) + \tilde{\mathbf{s}}_{\alpha;{\rm inel}}^{[2]}(z), \tag{B8}$$

where the two vectors

$$\tilde{\mathbf{s}}_{\alpha;{\rm el}}^{[2]}(z) \;=\; \frac{1}{z}\mathbf{G}_0\mathbf{V}\mathbf{G}_0\mathbf{j}\langle \sigma_{21}^\alpha \rangle_{\rm ss}^{[1]}, \tag{B9a}$$

$$\begin{aligned} \tilde{\mathbf{s}}_{\alpha;{\rm inel}}^{[2]}(z) \;=\; & \mathbf{G}_0(z)\mathbf{V}\mathbf{G}_0(z)\mathbf{s}_\alpha^{[1]}(0) + \mathbf{G}_0(z)\mathbf{s}_\alpha^{[2]}(0) \\ & + \frac{\langle \sigma_{21}^\alpha \rangle_{\rm ss}^{[1]}}{z}\left[\mathbf{G}_0(z)\mathbf{V}\mathbf{G}_0(z) - \mathbf{G}_0\mathbf{V}\mathbf{G}_0\right]\mathbf{j}, \end{aligned} \tag{B9b}$$

lead to the elastic and inelastic spectra, respectively.

Inserting (B9a) into (B6) we obtain

$$\begin{aligned} [\tilde{G}_{\rm ss}^{(1)}(z)]_{\rm el} \;=\; & \frac{1}{z}\Big(\langle \sigma_{21}^1\rangle_{\rm ss}^{[1]}\langle \sigma_{12}^1\rangle_{\rm ss}^{[1]} + \langle \sigma_{21}^2\rangle_{\rm ss}^{[1]}\langle \sigma_{12}^2\rangle_{\rm ss}^{[1]} \\ & + 2\,{\rm Re}\left\{\langle \sigma_{21}^1\rangle_{\rm ss}^{[1]}\langle \sigma_{12}^2\rangle_{\rm ss}^{[1]} e^{i\mathbf{k}\cdot\mathbf{r}_{12}}\right\}\Big), \end{aligned} \tag{B10}$$

with the right hand side expression in the round brackets being nothing but the stationary elastic intensity $I_2^{\rm el}$, Eq. (15). Finally, putting $[\tilde{G}_{\rm ss}^{(1)}(z)]_{\rm el}$ to (4) we arrive at

$$\tilde{I}_2^{\rm el}(\nu) = I_2^{\rm el}\delta(\nu), \tag{B11}$$

where we have used the formula

$$\lim_{\Gamma\to 0}\frac{1}{\Gamma - i\nu} = \pi\delta(\nu) + iP\frac{1}{\nu}, \tag{B12}$$

with P denoting the principal value of an integral.

One can check that the right hand side of Eq. (B9b) does not have a pole at $z = 0$, which means that the respective expression describes the inelastic spectrum.

2. Analytical results for inelastic spectrum at $\delta = 0$

a. Weak field ($\Omega \ll \gamma$)

At small Rabi frequencies, the analytical formulas are obtained after taking into account the lowest-order inelastic process – the two-photon scattering, – and neglecting the inelastic processes of higher orders. The two-photon processes are proportional to the square of the intensity, that is, to Ω^4. The ladder and crossed terms read (we omit the common prefactor $2|\bar{g}|^2/15$):

$$\tilde{L}_2^{\rm inel}(\nu) \;\simeq\; \frac{1}{\pi}\left(\frac{\Omega}{\gamma}\right)^4 \frac{\gamma^3(2\gamma^2 + \nu^2)}{2(\gamma^2 + \nu^2)^3}, \tag{B13}$$

$$\tilde{C}_2^{\rm inel}(\nu) \;\simeq\; \frac{1}{\pi}\left(\frac{\Omega}{\gamma}\right)^4 \frac{\gamma^5}{(\gamma^2 + \nu^2)^3}. \tag{B14}$$

It is easy to check that the expressions (B13), (B14) are consistent with the behavior of the enhancement factor in the two-photon scattering regime. Integrating $\tilde{L}_2^{\rm inel}(\nu)$, $\tilde{C}_2^{\rm inel}(\nu)$ over all frequencies, we obtain the following inelastic ladder and crossed terms for small Ω:

$$L_2^{\rm inel} = \int_{-\infty}^{\infty} d\nu \tilde{L}_2^{\rm inel}(\nu) = \frac{7}{16}\left(\frac{\Omega}{\gamma}\right)^4, \quad \text{(B15)}$$

$$C_2^{\rm inel} = \int_{-\infty}^{\infty} d\nu \tilde{C}_2^{\rm inel}(\nu) = \frac{3}{8}\left(\frac{\Omega}{\gamma}\right)^4. \quad \text{(B16)}$$

Combining Eqs. (B15), (B16) with the small-s expression for the elastic ladder and crossed terms $L_2^{\rm el} = C_2^{\rm el} = s$, and rewriting Eq. (B16) in terms of s, we recover the expected linear decrease

$$\alpha = 1 + \frac{s + 3s^2/2}{s + 7s^2/4} \simeq 2 - \frac{s}{4}. \quad \text{(B17)}$$

b. Strong field ($\Omega \gg \gamma$)

In the opposite limit of a strong field, the CBS intensity is inversely proportional to the laser field intensity. We will now present the analytical expressions for the ladder and crossed spectra derived in the leading order $\sim (\gamma/\Omega)^2$.

In this case, explicit expressions for CBS spectra can be represented by using a function of two real variables x_1 and x_2:

$$\pounds(x_1, x_2) = \frac{1}{\pi}\frac{x_1}{x_1^2 + x_2^2}. \quad \text{(B18)}$$

Let us mention the properties of $\pounds(x_1, x_2)$ that are important to us: (i) if $x_1 = \text{Const}$, then the function (B18) represents a Lorentzian with full width at half maximum (referred to as *width* in the main text) $2x_1$ and resonance at $x_2 = 0$; (ii) if $x_2 = \text{Const}$, then (B18) describes a resonance of a dispersive type at $x_1 = 0$, with the width $2x_2$.

With the help of the function (B18), the ladder and crossed spectra are given by

$$\begin{aligned}\tilde{L}_2^{\rm inel}(\nu) \simeq \left(\frac{\gamma}{\Omega}\right)^2 \Big(&\frac{1}{2}\pounds(\gamma,\nu) + \frac{1}{4}\pounds(3\gamma,\nu) \\ &+\frac{14}{9}[\pounds(3\gamma/2,\nu-\Omega/2) + \pounds(3\gamma/2,\nu+\Omega/2)] \\ &+\frac{1}{9}[\pounds(3\gamma/2,\nu-\Omega) + \pounds(3\gamma/2,\nu+\Omega)] \\ &+\frac{5}{18}[\pounds(5\gamma/2,\nu-\Omega) + \pounds(5\gamma/2,\nu+\Omega)] \\ &+\frac{1}{72}[\pounds(3\gamma,\nu-2\Omega) + \pounds(3\gamma,\nu+2\Omega)]\Big), \quad \text{(B19)}\end{aligned}$$

$$\begin{aligned}\tilde{C}_2^{\rm inel}(\nu) \simeq \left(\frac{\gamma}{\Omega}\right)^2 \Big(&\frac{1}{2}\pounds(2\gamma,\nu) + \frac{1}{4}\pounds(3\gamma,\nu) \\ &-\frac{1}{6}[\pounds(5\gamma/2,\nu-\Omega) + \pounds(5\gamma/2,\nu+\Omega)] \\ &+\frac{1}{72}[\pounds(3\gamma,\nu-2\Omega) + \pounds(3\gamma,\nu+2\Omega)]\Big) \\ &+\left(\frac{\gamma}{\Omega}\right)^3 \frac{208}{45} \\ &\times[\pounds(\nu+\Omega/2,3\gamma/2) - \pounds(\nu-\Omega/2,3\gamma/2)], \quad \text{(B20)}\end{aligned}$$

where the two terms of order $(\gamma/\Omega)^3$ are retained because they define dispersive resonances of $\tilde{C}_2^{\rm inel}(\nu)$ at $\nu = \pm\Omega/2$. By performing the elementary integrations of Eqs. (B19) and (B20) we arrive at the inelastic ladder and crossed terms

$$L_2^{\rm inel} \simeq \frac{14}{3}\left(\frac{\gamma}{\Omega}\right)^2, \quad C_2^{\rm inel} \simeq \frac{4}{9}\left(\frac{\gamma}{\Omega}\right)^2, \quad \text{(B21)}$$

which are consistent with Eqs. (A14), (A15) and, hence, with $\alpha = \alpha_\infty = 23/21$.

[1] D. V. Kupriyanov, I. M. Sokolov, C. I. Sukenik, and M. D. Havey, Laser Phys. Lett. **3**, 223 (2006).
[2] G. Labeyrie, F. de Tomasi, J.-C. Bernard, C. A. Müller, C. Miniatura and R. Kaiser, Phys. Rev. Lett. **83**, 5266 (1999).
[3] P. Kulatunga, C. I. Sukenik, S. Balik, M. D. Havey, D. V. Kupriyanov, and I. M. Sokolov, Phys. Rev. A **68**, 033816 (2003).
[4] E. Akkermans, G. Montambaux, J.-L. Pichard, and J. Zinn-Justin (Eds.) *Mesoscopic Quantum Physics* (Elsevier, Amsterdam, 1994).
[5] M. D. Lukin, Rev. Mod. Phys. **75**, 457 (2003).
[6] V. M. Datsyuk, I. M. Sokolov, D. V. Kupriyanov, and M. D. Havey, Phys. Rev. A **74**, 043812 (2006).
[7] S. E. Skipetrov, Phys. Rev. A **75**, 053808 (2007).
[8] T. Chanelière, D. Wilkowski, Y. Bidel, R. Kaiser, and C. Miniatura, Phys. Rev. E **70**, 036602 (2004).
[9] S. Balik, P. Kulatunga, C. I. Sukenik, M. D. Havey, D. V. Kupriyanov, and I. M. Sokolov, J. Mod. Opt. **52**, 2269 (2005).
[10] T. Jonckheere, C. A. Müller, R. Kaiser, C. Miniatura, and D. Delande, Phys. Rev. Lett. **85**, 4269 (2000).
[11] C. A. Müller, T. Jonckheere, C. Miniatura, and D. Delande, Phys. Rev. A **64**, 053804 (2001).
[12] C. A. Müller and C. Miniatura, J. Phys. A **35**, 10163 (2002).
[13] D. V. Kupriyanov, I. M. Sokolov, P. Kulatunga, C. I. Sukenik, and M. D. Havey, Phys. Rev. A **67**, 013814 (2003).
[14] G. Labeyrie, D. Delande, C. A. Müller, C. Miniatura, and R. Kaiser, Europhys. Lett. **61**, 327 (2003).
[15] Y. Bidel, B. Klappauf, J. C. Bernard, D. Delande, G. Labeyrie, C. Miniatura, D. Wilkowski, and R. Kaiser, Phys. Rev. Lett. **88**, 203902 (2002).
[16] T. Wellens, B. Grémaud, D. Delande, and C. Miniatura, Phys. Rev. A **70**, 023817 (2004).

[17] T. Wellens, B. Grémaud, D. Delande, and C. Miniatura, Phys. Rev. E **71**, 055603(R) (2005).
[18] T. Wellens, B. Grémaud, D. Delande, and C. Miniatura, Phys. Rev. A **73**, 013802 (2006).
[19] V. Shatokhin, C. A. Müller, and A. Buchleitner, Phys. Rev. Lett. **94**, 043603 (2005).
[20] V. Shatokhin, C. A. Müller, and A. Buchleitner, Phys. Rev. A **73**, 063813 (2006).
[21] B. Grémaud, T. Wellens, D. Delande, C. Miniatura, Phys. Rev. A **74**, 033808 (2006).
[22] V. Shatokhin, Opt. Spectrosc. **103**, 300 (2007); preprint arXiv:quant-ph/0608094 (2006).
[23] R. J. Glauber, in *Quantum Optics and Electronics*, edited by C. DeWitt, A. Blandin, and C. Cohen-Tannoudji (Gordon and Breach, London, 1965).
[24] M. O. Scully and M. S. Zubairy, *Quantum Optics*, (Cambridge University Press, Cambridge, U. K., 1997).
[25] R. H. Lehmberg, Phys. Rev. A **2**, 883 (1970).
[26] B. R. Mollow, Phys. Rev. **188**, 1969 (1969).
[27] J. H. Shirley, Phys. Rev. **138**, B979 (1965).
[28] C. Cohen-Tannoudji, J. Dupont-Roc, G. Grynberg, *Atom-Photon Interactions* (Wiley, New York, 1992).
[29] R. W. Boyd, *Nonlinear optics* (Academic, San Diego, 1992).
[30] S. H. Autler and C. H. Townes, Phys. Rev. **100**, 703 (1955).
[31] B. R. Mollow, Phys. Rev. A **5**, 1522 (1972).
[32] V.N. Shatokhin and S.Ya. Kilin, Phys. Rev. A **63**, 023803 (2001).
[33] D.V. Kupriyanov, I.M. Sokolov, and M.D. Havey Opt. Commun. **243**, 165 (2004).